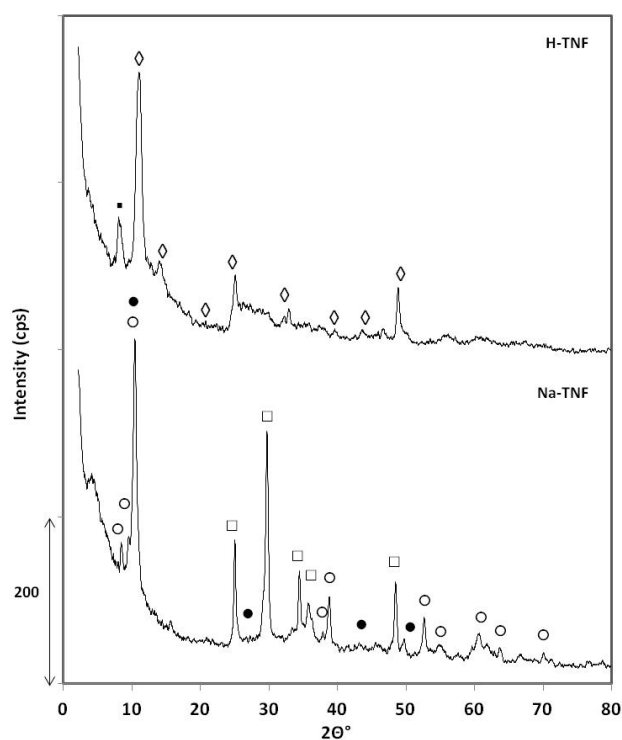


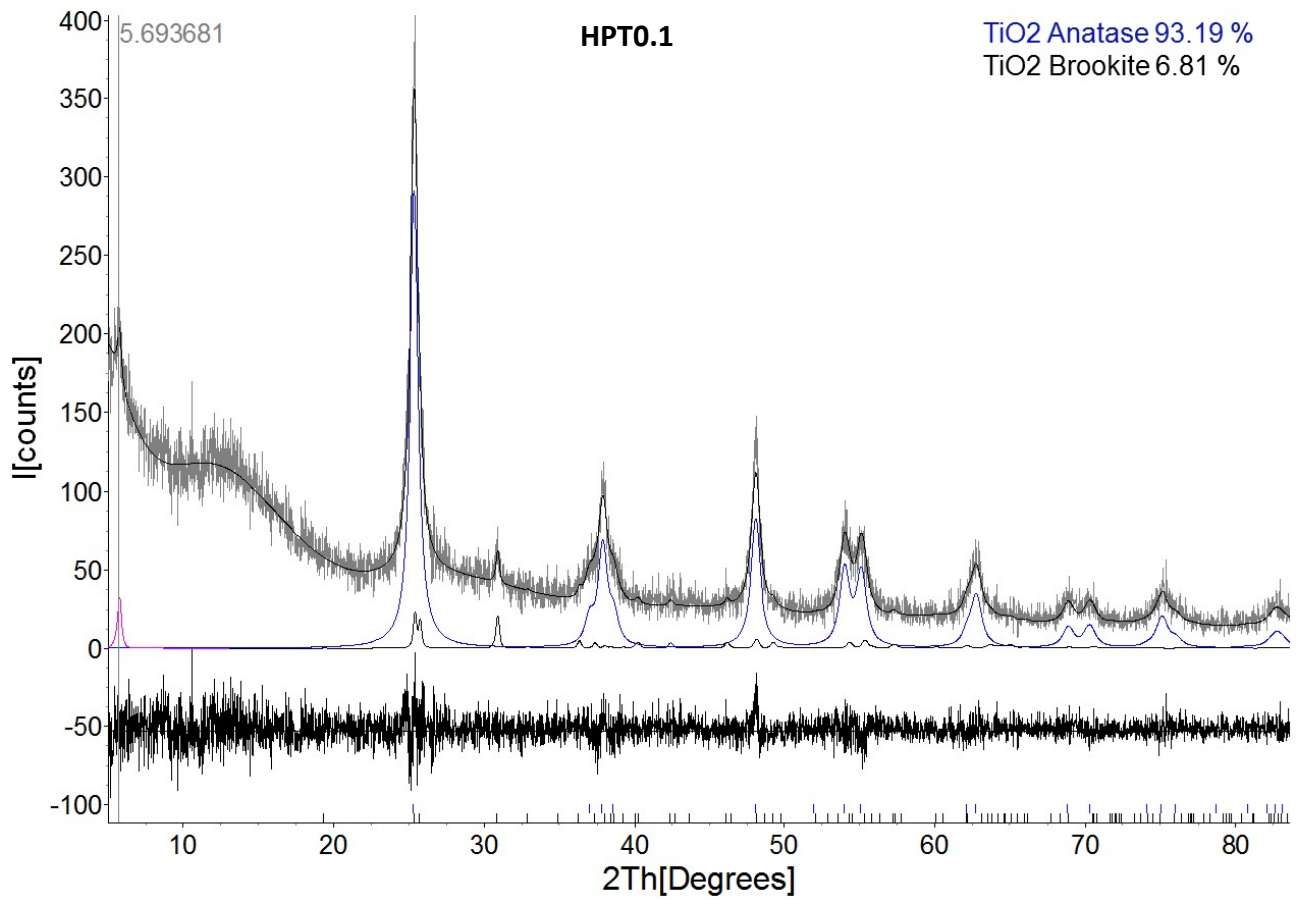
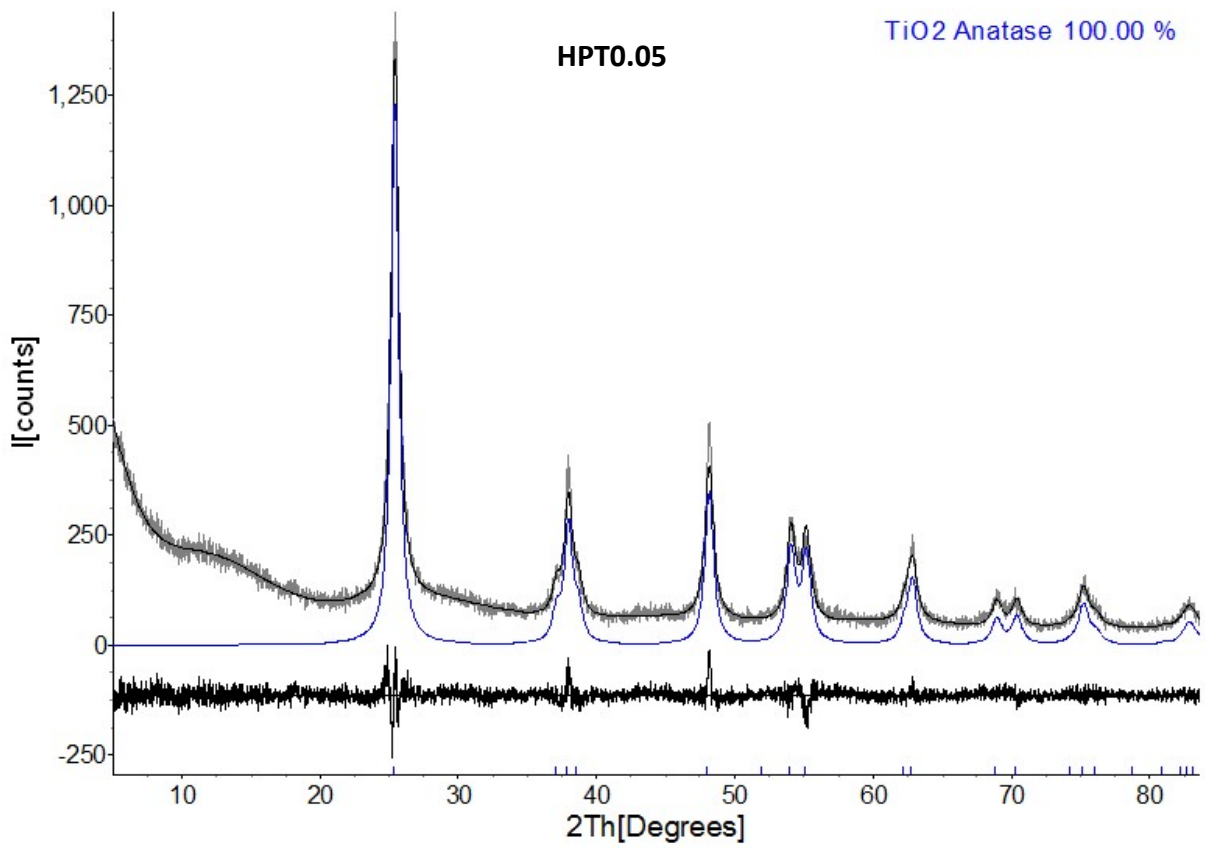
Supporting Information

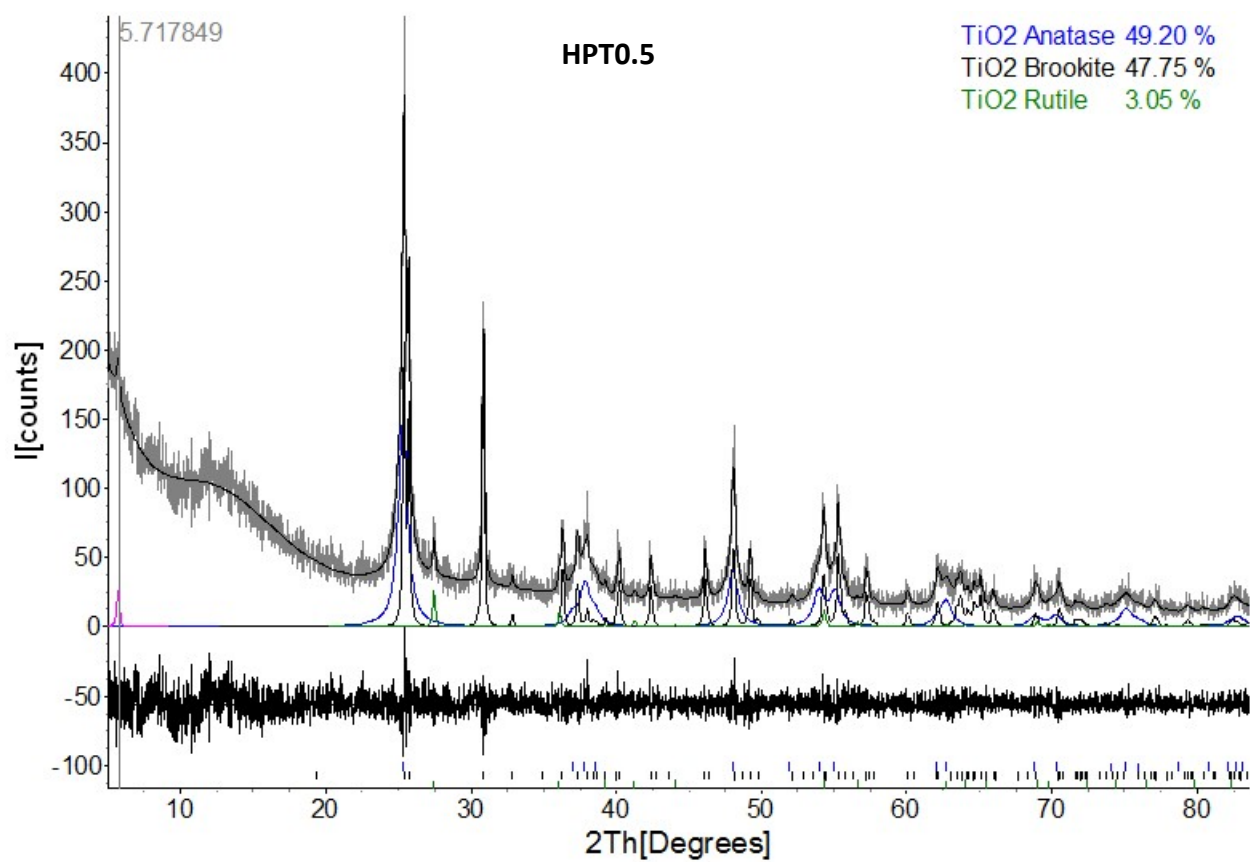
New Insights into the Relationship between Structure and Photocatalytic Properties of TiO₂ Catalysts

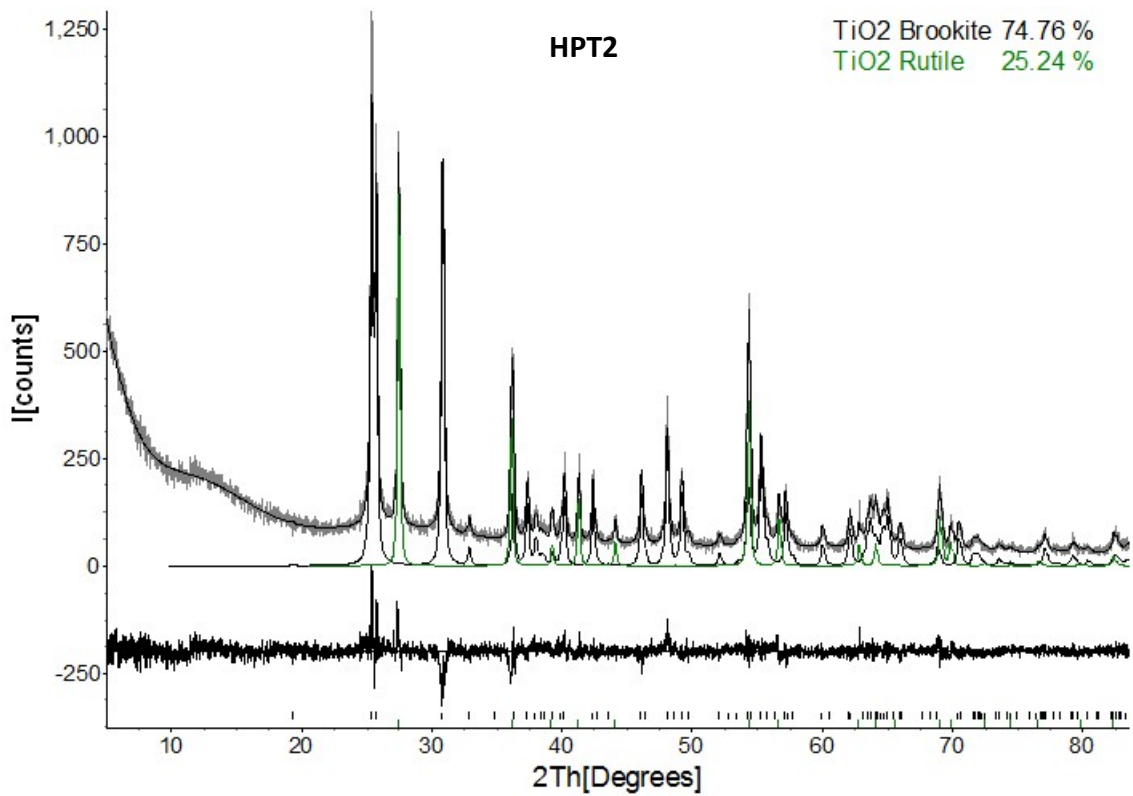
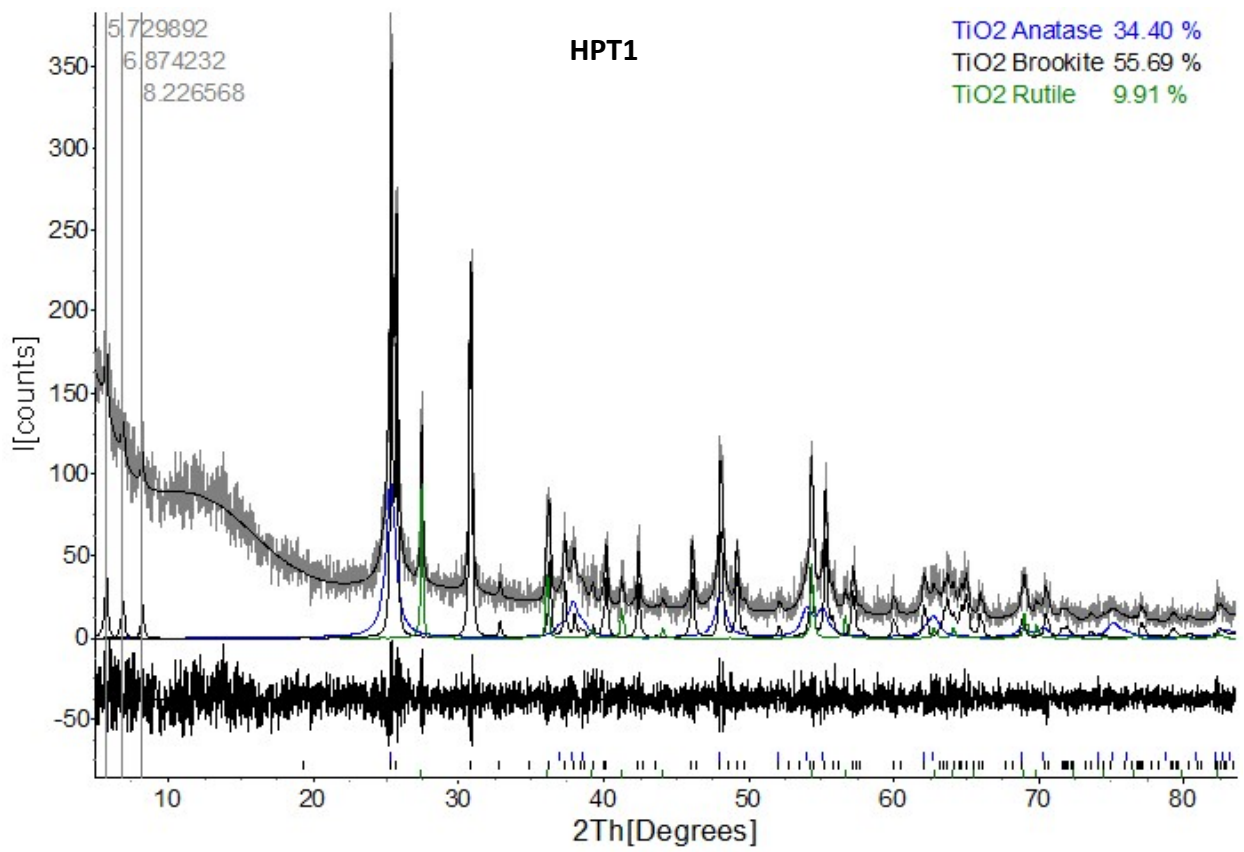
Ágnes Veres, Judit Ménesi, Csaba Janáky, Gergely F. Samu, Martin Karl Scheyer, Qisong Xu, Fatma Salahioğlu, Marc V. Garland, Imre Dékány,* Ziyi Zhong*

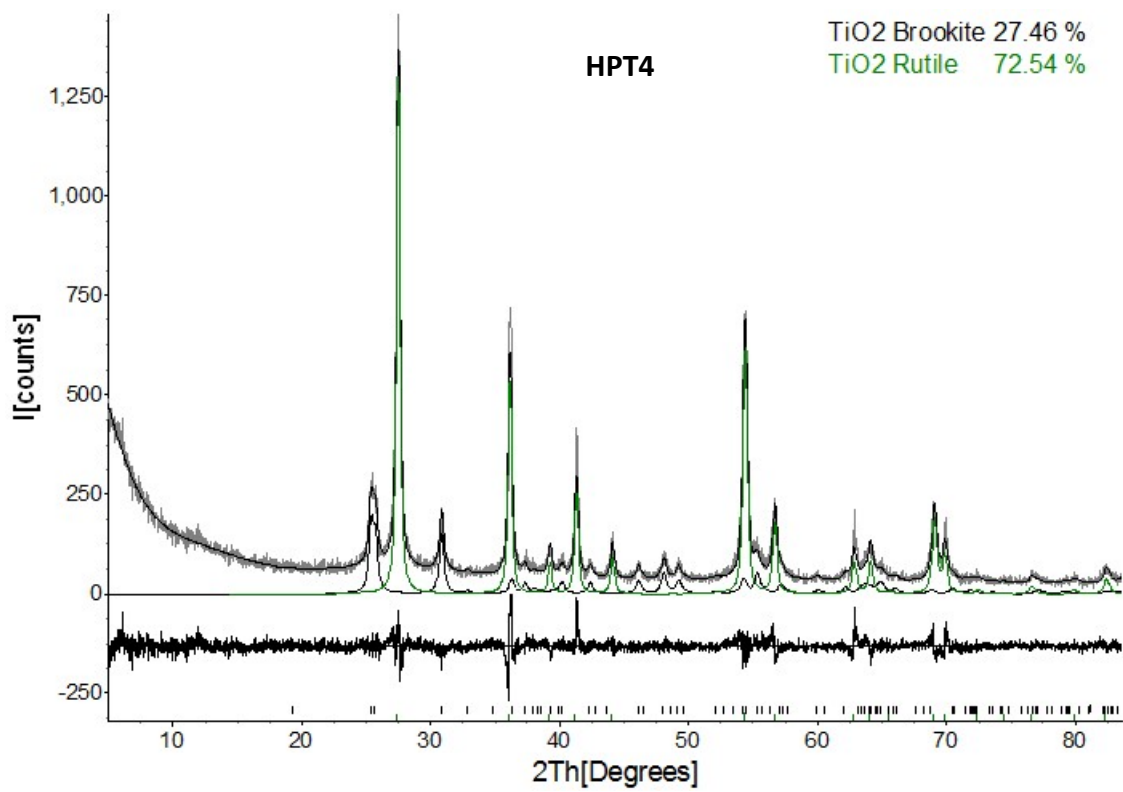


SI Figure 1 XRD patterns of hydrothermal products: Na-TNF before, and H-TNF after washing with HCl. ○ – Na₂Ti₃O₇; ● – Na₂Ti₄O₉; □ – Na₂Ti₉O₁₉ and ◇ H₂Ti₂O₇, and ■ H₂Ti₅O₁₁ · 3·H₂O.

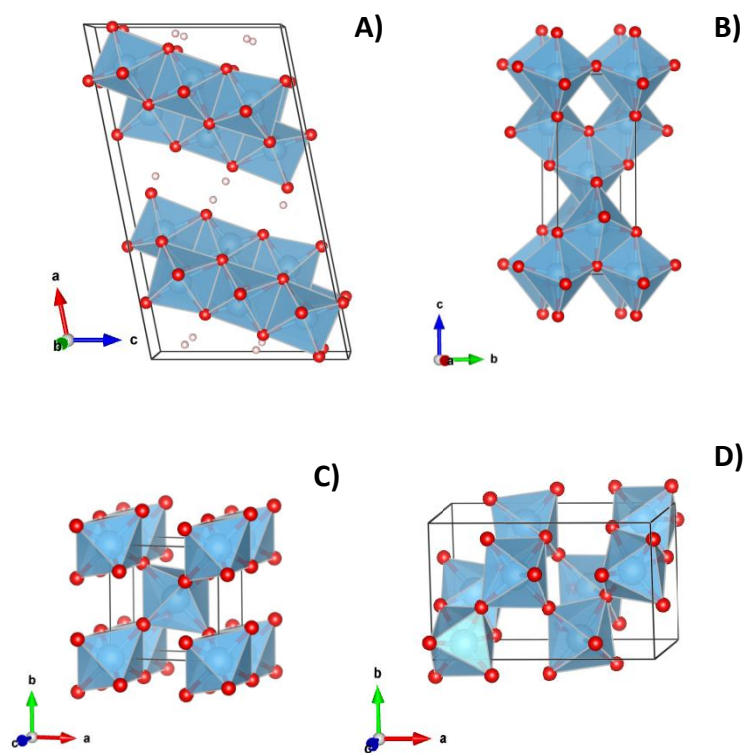








SI Figure 2 Rietveld refinements of the TiO₂ samples.

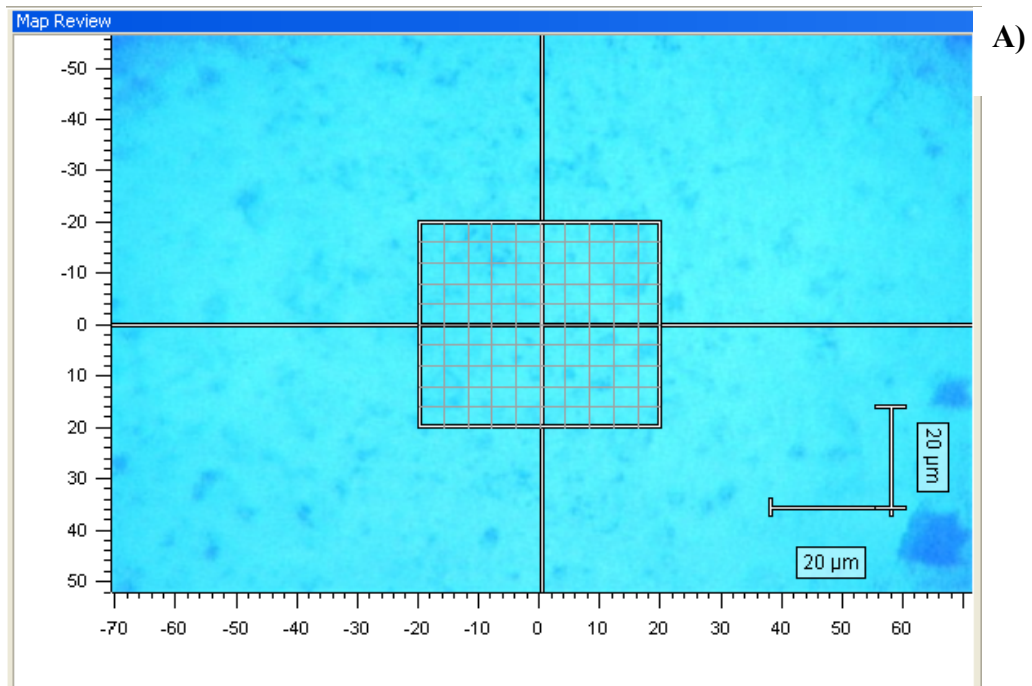


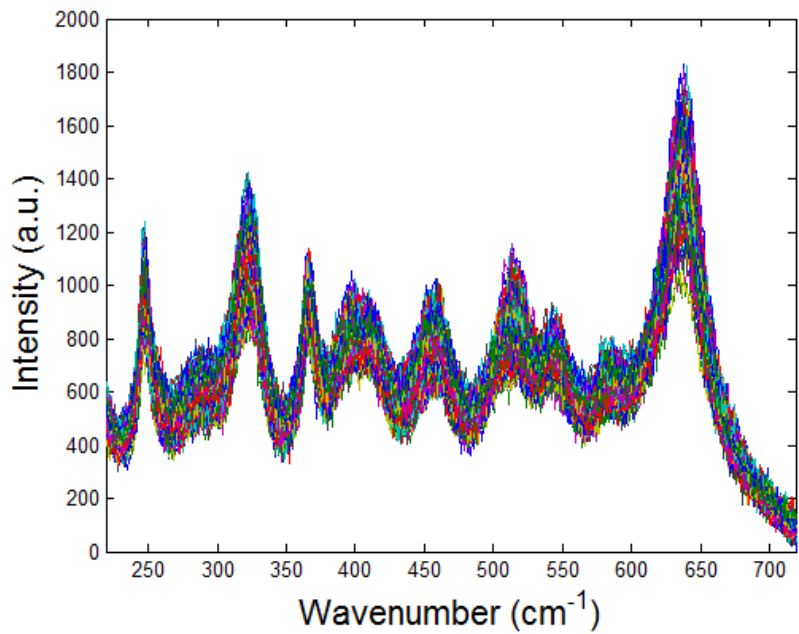
SI Figure 3 Crystal structures of **A)** $\text{H}_2\text{Ti}_3\text{O}_7$; **B)** anatase; **C)** brookite and **D)** rutile, illustrated by VESTA visualisation program (K. Momma, F. Izumi, *J. Appl. Crystallogr.* 2011, **44**, 1272.)

Experimental details on Raman measurement combined with BTEM and generated concentration maps of the polymorphs

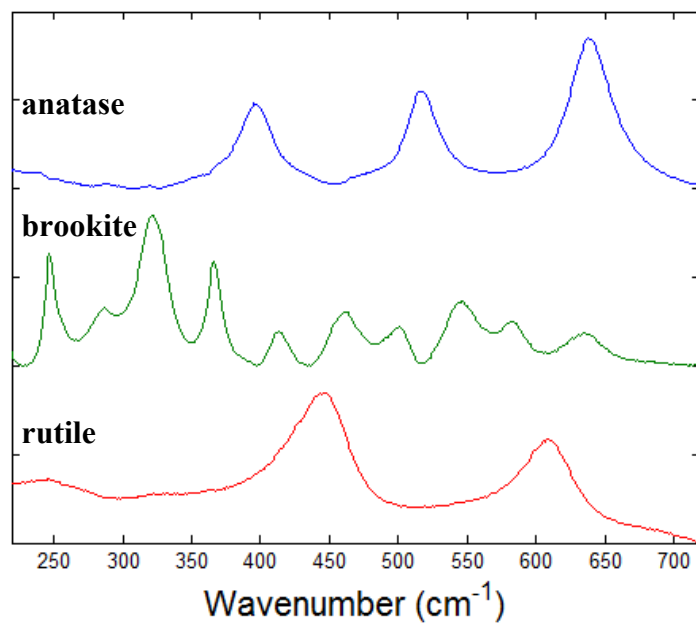
Raman measurements combined with BTEM[®] algorithms for signal processing were first carried out as a complementary measurement to PXRD. However, using this chemometric tool additional, unexpected information was also revealed about the crystalline nature of the TiO_2 samples. This state-of-the-art method has the ability of working with a huge dataset and to reconstruct the estimated pure component spectra without the use of any *a priori* information, even from data with very low signal-to-noise ratio^{1,2}. Here, it gave us the advantage of monitoring the distribution of polymorphs in the bulk. An area of $1600 \mu\text{m}^2$ of the TiO_2 powders was scanned by Raman microscopy to analyze the crystal phase composition of the powders (**SI Figure 4A**). Before the Raman measurements, the powders were well grounded in a mortar and mixed with a spatula to homogenize then they were pressed into pellets. This latter step was important to create a relatively smooth surface in order to minimize the Raman signal intensity differences. Assuming that the penetration energy of laser light of the Raman microscope was $3\text{-}5 \mu\text{m}$, we had representative volume of $4800\text{-}8000 \mu\text{m}^3$ of the sample for data collection. The collected large number of Raman spectra (**SI Figure 4B**) were first reconstructed into the estimated pure components (**SI Figure 4C**) then mapped into the original spectra to obtain the relative concentrations of various TiO_2 phases (**SI Figure 5-9**). Subsequently, the calculated data were organized to obtain the spatial distribution of the crystalline phases, representative for the scanned area. In each data point of the concentration map, the relative estimated amount of respective crystal phases were presented. By expressing the relative calculated values instead of the absolute estimated values; the error, originating from intensity differences of the signal due to minor roughness or height difference of the surface was cancelled out. It was found that anatase and brookite phases showed fairly even distribution along the scanned area in HPT0.1 (**SI Figure 5**). A minor amount of rutile (3.05%), determined from PXRD data by Rietveld refinement,

first appeared in sample HPT0.5. A dark red spot, obtained on the top right quarter of the concentration maps, indicated that the local concentration of rutile/brookite and rutile/anatase was increased compared to those measured for the rest of the recorded data points (**Figures 6 A and B, respectively**). With further increase of the acid concentration, not only the amount of rutile was increasing (the magnitude of scale bar is a good indicator of that), but the inhomogeneous phase distribution was also more and more observable for HPT1; HPT2 and HPT4. With other words; the more rutile was formed in the samples, the less homogeneity was achieved for the spatial distribution of the respective polymorphs. As a consequence of phase separation, there were less heterojunctions expected to be present.



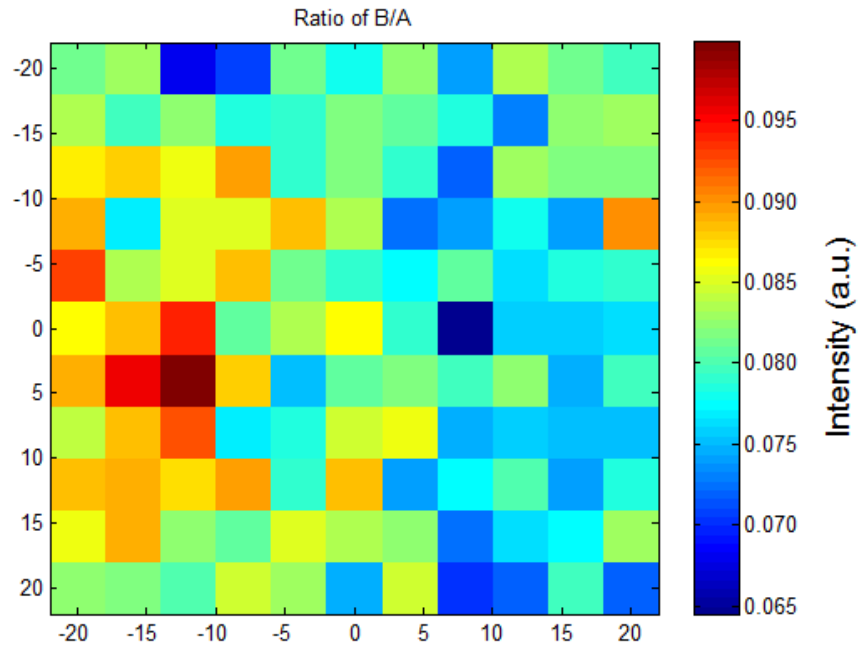


B)

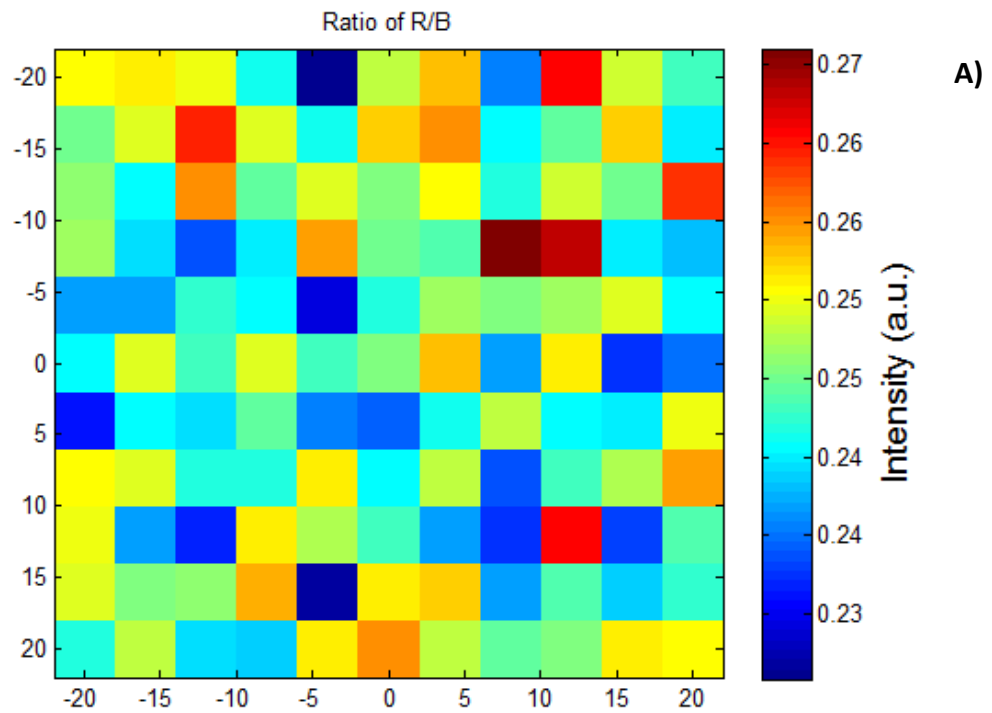


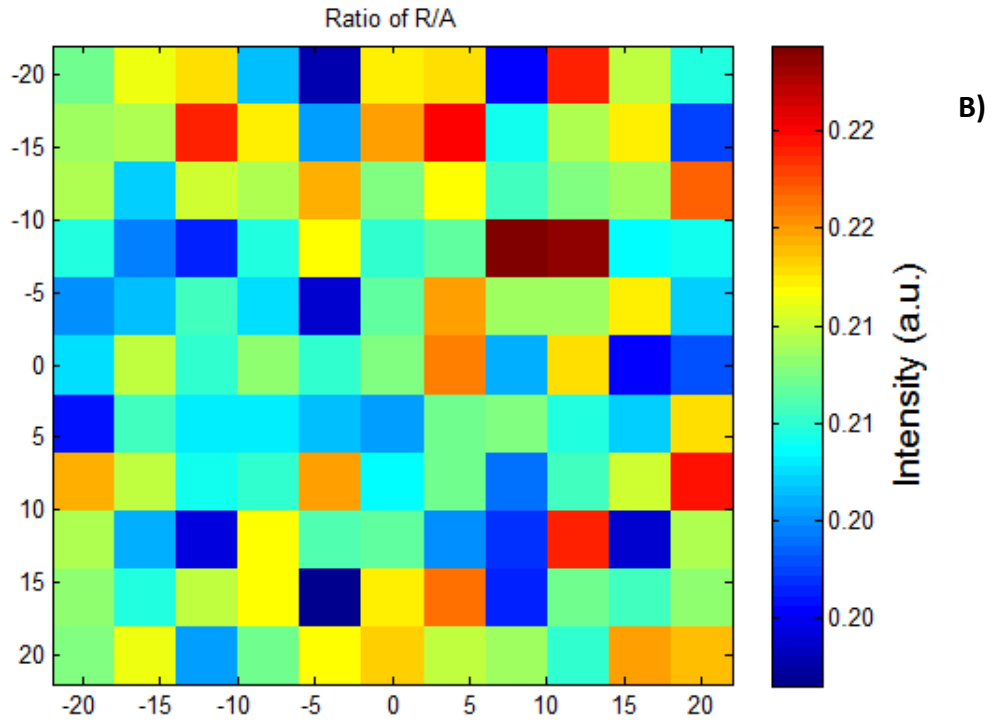
C)

SI Figure 4 A) A microscopic view and **B)** recorded raw Raman signals for HPT1. **C)** Estimated pure component spectra of anatase, brookite and rutile reconstructed from raw signals, recorded in one data point for HPT1

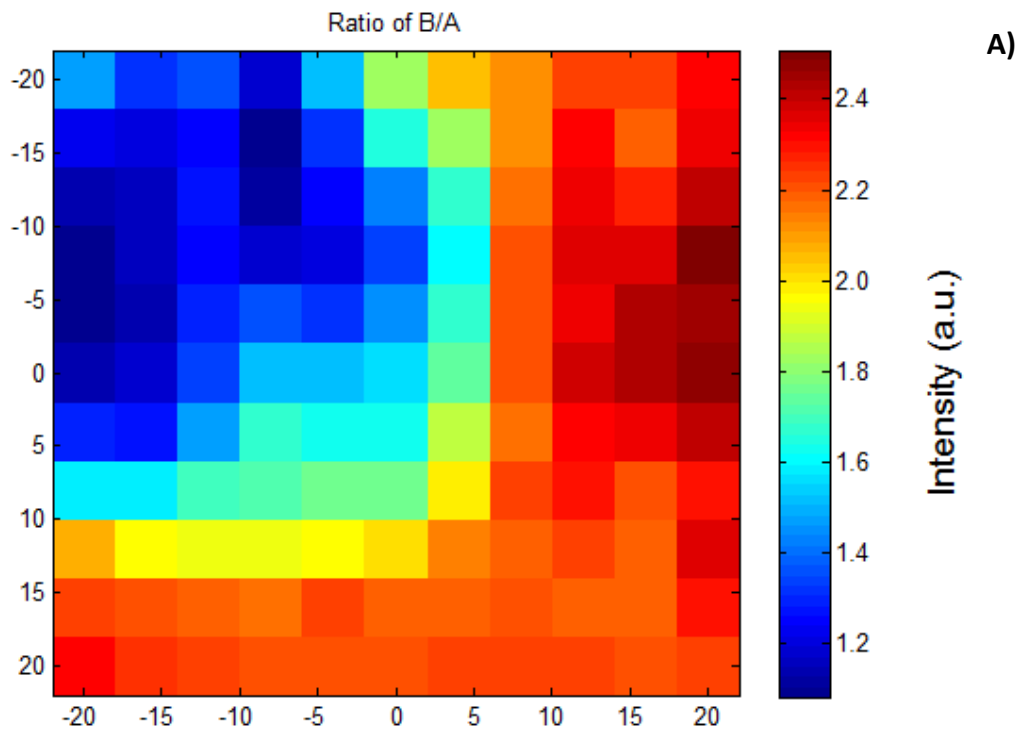


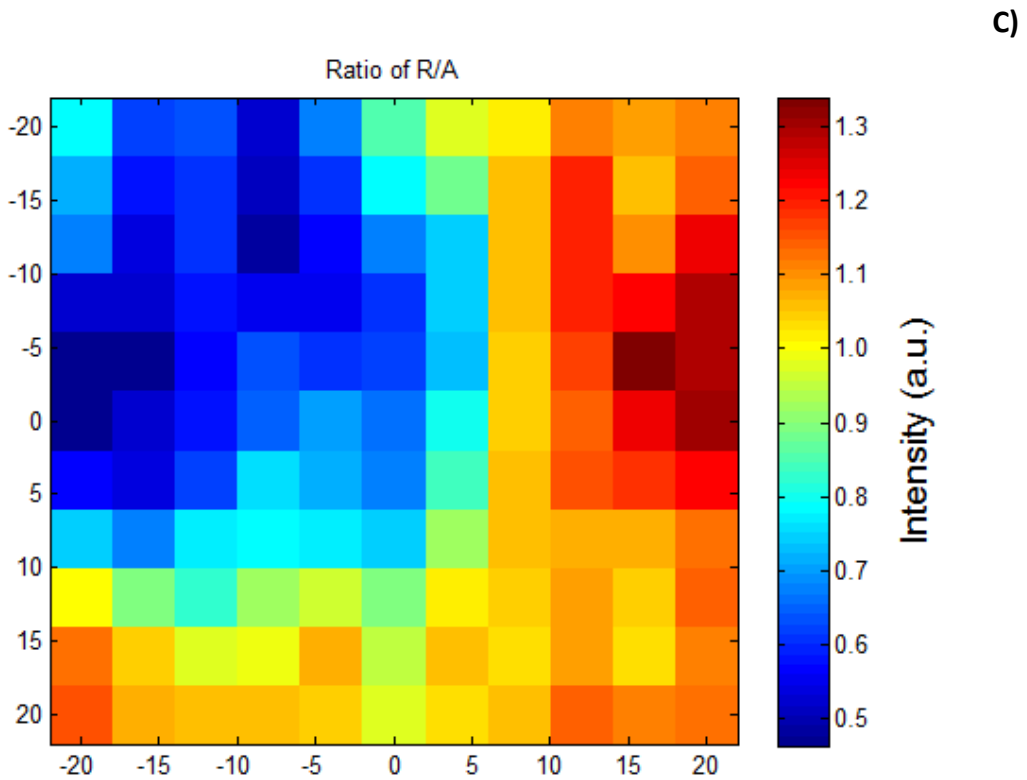
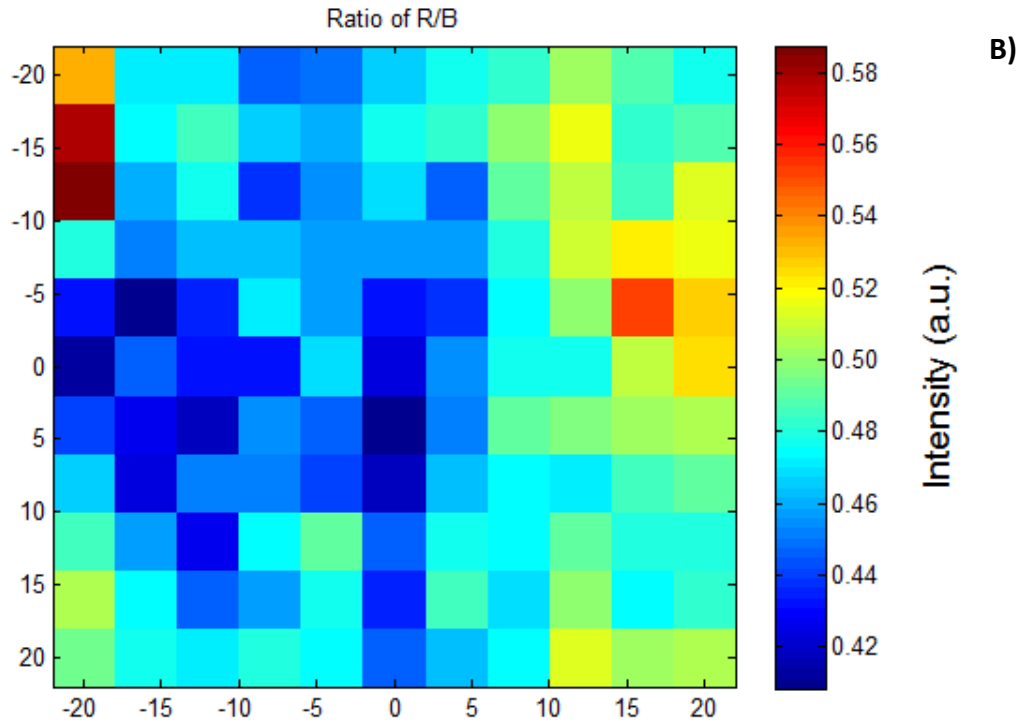
SI Figure 5 Concentration map of HPT0.1 showing the calculated relative amounts of brookite/anatase phases



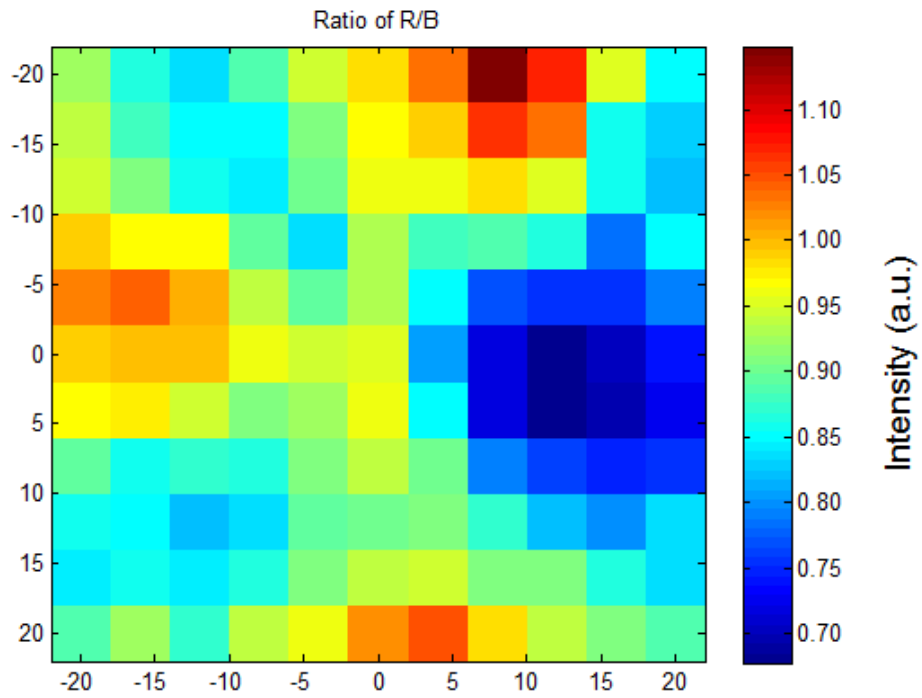


SI Figure 6 Concentration map of HPT0.5 showing calculated relative amounts of **A)** rutile/brookite and **B)** rutile/anatase phases

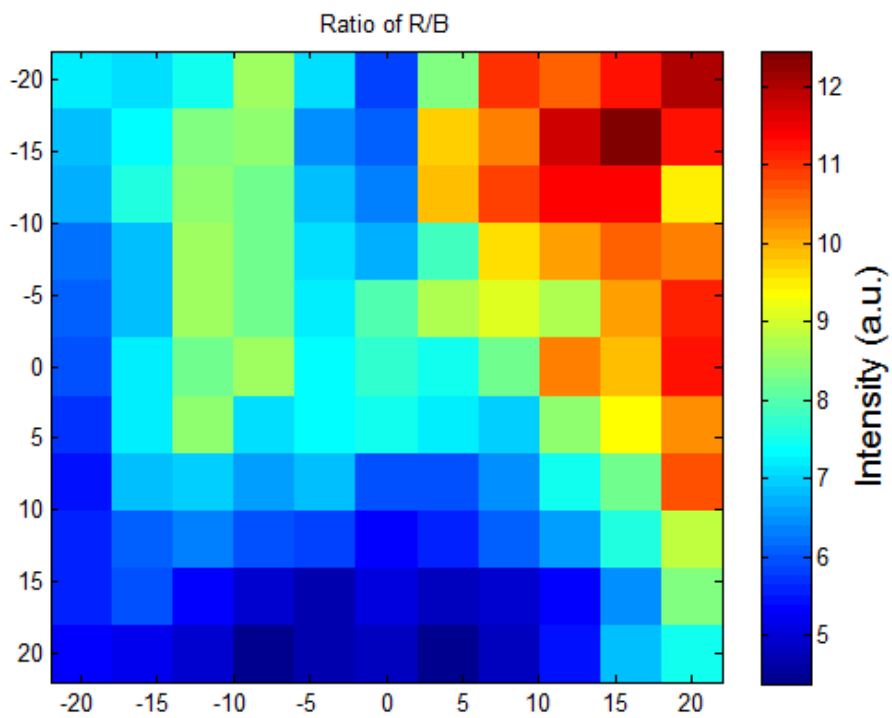




SI Figure 7 Concentration maps of HPT1 showing relative amounts of **A)** brookite/anatase, **B)** rutile/brookite phases and **C)** rutile/anatase phases



SI Figure 8 Concentration map of HPT2 showing relative amounts of rutile/brookite phases



SI Figure 9 Concentration map of HPT4 showing relative amounts of rutile/brookite phases

References

- ¹ E. W. M. G. W. Chew, "Band-Target Entropy Minimisation (BTEM): An advanced method for recovering unknown pure component spectra. Application to the FTIR spectra of unstable organometallic mixtures," *Organometallics*, vol. 9, pp. 1982-1990., 2002.
- ² M. G. E. Widjaja, "Detailed spectroscopic analysis of complex multi-component materials using a combination of Raman mapping with BTEM," *J. Raman Spectrosc.*, vol. 43, pp. 828-833., 2012.